Published in final edited form as:
Cell. 2011 July 8; 146(1): 164–176. doi:10.1016/j.cell.2011.06.016.

Assembly of lamina-specific neuronal connections by Slit bound to type IV Collagen

Tong Xiao[1], **Wendy Staub**[1], **Estuardo Robles**[1], **Nathan J. Gosse**[1], **Gregory J. Cole**[2], and **Herwig Baier**[1]

[1]University of California, San Francisco, Department of Physiology, Programs in Neuroscience, Genetics, and Developmental Biology,1550 Fourth Street, San Francisco, California 94158-2722

[2]North Carolina Central University, Julius L. Chambers Biomedical/Biotechnology Research Institute, 700 George Street, Durham, NC 27707

Abstract

The mechanisms that generate specific neuronal connections in the brain are under intense investigation. In zebrafish, retinal ganglion cells project their axons into at least six layers within the neuropil of the midbrain tectum. Each axon elaborates a single, planar arbor in one of the target layers and forms synapses onto the dendrites of tectal neurons. We show that the laminar specificity of retinotectal connections does not depend on self-sorting interactions among RGC axons. Rather, tectum-derived Slit1, signaling through axonal Robo2, guides neurites to their target layer. Genetic and biochemical studies indicate that Slit binds to Dragnet (Col4a5), a type IV Collagen, which forms the basement membrane on the surface of the tectum. We further show that radial glial endfeet are required for the basement-membrane anchoring of Slit. We propose that Slit1 signaling, perhaps in the form of a superficial-to-deep gradient, presents laminar positional cues to ingrowing retinal axons.

Keywords

Slit1; Slit2; Robo2; Col4a5; Ext2; Extl3; visual system; retinal ganglion cell; tectum; superior colliculus; lamination; axon; dendrite; radial glia; retinotectal; retinocollicular; heparan sulfate proteoglyan; HSPG; synaptic specificity

Introduction

Synaptic connections with similar functions are often organized in layers. This anatomical principle is most evident in the cortex, hippocampus, retina, tectum (superior colliculus) and spinal cord of vertebrates and in the optic lobes of *Drosophila* (Huberman et al., 2010; Sanes and Yamagata, 2009). The optic tectum of larval zebrafish is an excellent model system to investigate the development and function of lamina-specific connections (Nevin et al., 2010). Axons of retinal ganglion cells (RGCs) make contacts with tectal dendrites in a dense neuropil region that is surrounded on three sides by cell bodies and covered by a sheet of basement membrane (Xiao and Baier, 2007). Radial glia are oriented perpendicular to the

Correspondence should be addressed to H. B. (herwig.baier@ucsf.edu)..

laminae and span the entire depth of the tectum. These cells extend processes with a `bottlebrush' morphology to the neuropil surface, where they are anchored to the basement membrane through their endfeet (Halfter and Schurer, 1998; Halfter et al., 2002). Radial glia have been implicated in supporting the layered architecture of the brain by virtue of their morphology and their intimate contacts with migrating cells (Rakic, 2003), but their exact signaling function remains unclear.

RGC axons project to at least four major strata at the surface of the tectum: the *stratum opticum* (SO), right beneath the basement membrane, and three sublaminae of the *stratum fibrosum griseum et superficiale* (named $SFGS_B$, $SFGS_D$, and $SFGS_F$ from superficial to deep) (Xiao et al., 2005). Individual RGCs innervate just one tectal (sub-)lamina. Their axons branch extensively to form a flat terminal arbor within the plane of the target lamina (Xiao and Baier, 2007; Nevin et al., 2011). Laminar specificity of an RGC axon is determined by its subtype identity (Huberman et al., 2008; Huberman et al., 2009; Xiao et al., 2005; Yamagata and Sanes, 1995b). Tectal neurons are diverse in their morphologies and extend monostratified, multistratified, or diffuse dendritic arbors into the neuropil, where some of them receive inputs from RGC axons (Nevin et al., 2010; Robles et al., 2011; Scott and Baier, 2009).

While the retinotopic mapping of RGC axons along the anterior-posterior and dorsalventral coordinates of the tectum has been extensively studied in zebrafish (e. g., Baier et al., 1996) and other vertebrates (Lemke and Reber, 2005), little is known about the mechanisms directing axons and dendrites to their layers along the superficial-to-deep axis. Tectal laminae express specific markers, including cell-adhesion molecules that may serve as recognition cues for ingrowing neurites expressing the complementary receptors (Inoue and Sanes, 1997; May, 2006; Nevin et al., 2008). However, it is clear that the stereotypical order of neuropil layers cannot be explained by cell-to-cell surface interactions alone. Rather, it seems likely that the nascent neuropil is pre-patterned early in development by a vertical coordinate system that guides axons and/or dendrites to appropriate levels.

Slits are secreted glycoproteins, which bind and activate Robo receptors (Brose et al., 1999; Kidd et al., 1999; Li et al., 1999). Slit/Robo signaling plays important roles in axon guidance in the spinal cord. In the retinotectal projection of vertebrates, Robo2 is expressed by RGCs and directs the growth of axons in response to Slit1 and Slit2 expressed in cells that border the optic tract (Erskine et al., 2000; Fricke et al., 2001; Hutson and Chien, 2002; Plump et al., 2002). In addition, Robo2 appears to be a negative regulator of axon arbor formation and synaptogenesis in the zebrafish tectum (Campbell et al., 2007). Here we show that Slit/Robo signaling is also crucial for lamina-specific targeting of retinotectal connections. We provide evidence for surface localization of Slit by Collagen IV and radial glial endfeet, likely giving rise to a steep gradient that guides SFGS-projecting axons to the appropriate depth within the tectal neuropil. To our knowledge, this is the first demonstration of an extracellular guidance system organizing synaptic lamination in the brain.

Results

Transgenic reporters reveal the layered architecture of the retinotectal projection

The *Pou4f3:Gal4*-expressing subpopulation of RGCs innervates SO, $SFGS_D$, and $SFGS_F$. We asked whether the stratification patterns of tectal dendrites match these retinorecipient layers. In *Tg*(*Dlx5/6:GFP*) transgenic fish (Ghanem et al., 2003), a small subset of tectal neurons are labeled (Robles et al., 2011). Neurites from these tectal neurons extend to SO, two sublaminae of SFGS ($SFGS_B$ and $SFGS_D$) and deeper layers not innervated by RGCs (Fig. 1A). Two of these layers (SO and $SFGS_D$) overlap with the *Pou4f3:Gal4* and *UAS:mmCherry* labeled RGC axons (Fig. 1B,C).

To visualize the morphologies and stratification patterns of individual neurons, we employed a mosaic labeling technique described previously. The highly variegated *UAS:mGFP* contained within the *Tg*(*pou4f3c:Gal4, UAS:mGFP*)^{s318t} (*BGUG*) transgene was crossed into the *Gal4s1013t* enhancer trap line, which drives expression in most tectal neurons (Scott and Baier, 2009). At 6 dpf, almost half (40%) of single tectal neurons labeled with this technique showed clear lamina-specific projections (Scott and Baier, 2009; example in Fig. 1D). Tectal neurons are either mono- or bistratified, i. e., their neurites are restricted to one or two laminae, or they have diffuse arbors. In addition, we observed radial glial cells with their distinctive `bottlebrush' morphologies (Fig. 1E). These cells become GFAP-positive at 8 dpf and extend through all the layers, with their somata residing in the periventricular layer and their club-shaped endfeet attached to the surface of the neuropil. Together, our survey of single-cell stratification patterns revealed a highly organized, layered architecture of cellular processes in the zebrafish tectum (Fig. 1F).

Lamina-specific guidance depends exclusively on axon-target interactions

We considered the possibility that an individual RGC axon might target its layer based on selective fasciculation or repulsive interactions with other RGC axons. Wildtype (WT) cells, carrying the *Pou4f3:mGFP* transgene (Xiao et al., 2005), were transplanted into a *lakritz* (*lak*^{th241}) mutant host to generate chimeras containing single RGCs in an otherwise RGC-depleted background. *lak* mutants do not generate RGCs due to a null mutation in the proneural transcription factor Atoh7 (Kay et al., 2001). This defect is cell-autonomous; WT cells in a *lak* host may still differentiate into RGCs (Kay et al., 2005; Poggi et al., 2005). The *atoh7* gene is not expressed in the tectum or along the optic tract, and tectal cells do not seem to be affected by the absence of retinal input in their morphologies and relative frequencies (Gosse et al., 2008).

From several thousand WT –> *lak* chimeras, we selected 52 cases in which solitary, GFP-labeled RGC axons could be observed in the tectum and analyzed their laminar position in the tectal neuropil. We noticed that almost all single RGC axons (51 of 52, or 98%) targeted a single layer regardless of whether they were transplanted into a WT or a *lak* host (Fig. 1G, H). The proportions of axons projecting to SO vs. SFGS were not significantly different between the RGC-depleted vs. the crowded (WT) condition (Fig. 1K). This finding indicated that axon-axon interactions are not required and that axon-tectum interactions are sufficient for lamina-specific axon targeting. Axon guidance cues and their receptors are frequently expressed both by axons and their targets. The single-axon autonomy observed here thus reduces the complexity of candidate molecular signaling events.

Robo2 signaling is required for axonal laminar targeting

We reasoned that gradients or bands of secreted molecules, deposited in the ECM, could impart laminar positional information on the tectal neuropil. Axon guidance molecules of the Slit family are expressed in the tectum and are known to influence RGC axon growth in zebrafish (Campbell et al., 2007). Robo2 functions as the receptor for both Slit1 and Slit2 (Brose et al., 1999) and is disrupted in *astray* (*ast*^{ti272z}) mutants (Fricke et al., 2001). Although the vertebrate genome contains at least three *robo* genes, *robo2* is the only family member expressed by RGCs (Lee et al., 2001).

A subset of the RGC axons in *ast*^{ti272z} mutants fail to cross midline at the optic chiasm and instead project aberrantly to other brain areas (Suppl. Fig. S1), as reported previously (Fricke et al., 2001). The remaining, tectum-innervating axons make severe laminar-targeting errors. Rather than projecting exclusively to SO, $SFGS_D$, or $SFGS_F$, as *Pou4f3:mGFP* axons do in WT, axons in all mutant animals examined (n=6) are found broadly at most vertical positions within the tectal neuropil (Fig. 2A–C). We analyzed the

trajectories of single *ast*^{ti272z} mutant axons in the *BG/BGUG* double-transgenic background, in which a random subset of five to twenty RGC axons are labeled due to position-effect mosaicism (Xiao and Baier, 2007). In WT, RGC axons innervate and arborize in one lamina (Fig. 2D). In contrast, in *ast*^{ti272z}, the RGC axons meander between laminae (Fig. 2E, F) (*n*=24). This result demonstrated a requirement for Robo2 in laminar pathfinding in the tectum.

Slit1a is required for lamina-specific targeting in the tectum

Slit1a is the only known Slit family member expressed by tectal cells in zebrafish (Suppl. Fig. S2A). Slit2 is expressed by cells outside the tectum (Suppl. Fig. S2B). We analyzed embryos injected with antisense morpholino oligonucleotides (MO) to knock down either *slit1a* or *slit2*. High doses of either MO induced heart edema before 3 dpf and led to sickness (Suppl. Table 1). For imaging, we selected only larvae with apparently normal morphology (which had presumably received a lower dose of MO). Whilst control MOs (random standard control) had no effect on *pou4f3:mGFP* labeled retinal axons (Fig. 2G), *slit1a* morphant axons projected more broadly across the neuropil (Fig. 2H; summarized in Fig. 2I). In controls, single BGUG-labeled retinal axons remain strictly laminated (Fig. 2J). With *slit1a* MOs, axons were observed meandering through different layers (*n*=23 out of 25 imaged embryos) (Fig. K, L). Knockdown of *slit2* did not change axon targeting (Suppl. Table 1).

We compared the laminar targeting defect caused by *slit1a* knockdown with that seen in *ast*^{ti272z} mutants by measuring the depth of the *pou4f3:mGFP*-labeled retinal projections in the tectal neuropil (Fig. 2S; Suppl. Fig. S1D, E, F). In WT embryos, *pou4f3:mGFP* RGC axons occupy the superficial 60% of the neuropil; the deeper layers, 40% of the neuropil's thickness, are not innervated by this axon population. In both *ast*^{ti272z} mutants and *slit1a* MOs, *pou4f3:mGFP* RGC axons are found both in the superficial and deep layers (90% and 80% of the neuropil's thickness, respectively). Single axons in *ast*^{ti272z} mutants and *slit1a* MOs are also similar in their `thickness', i. e., they spread more broadly in the neuropil than controls (Fig. 2T). Therefore, Slit1a is the endogenous ligand of RGC-expressed Robo2 and is required for axon targeting in the tectum.

Overexpression of Slit disrupts lamina-specific targeting

We took advantage of an *hsp70l:Slit2-GFP* transgenic fish to overexpress Slit at various embryonic stages (Yeo et al., 2001). (A Slit1a-OE transgenic line was not available to this study; biochemically, both Slit1 and Slit2 act as apparently interchangeable Robo2 ligands; Brose et al., 1999). Slit2 is proteolytically cleaved between the EGF5 and EGF6 motifs *in vivo* (Yeo et al., 2001). Therefore, in the Slit2-OE embryos, the biologically active Slit-N is cleaved from inactive Slit2-C, which is fused with GFP. Degradation of Slit2-C-GFP over the ensuing days enabled us to image *Pou4f3:mGFP* axons in the heat-shocked fish. We established that transgenically expressed Slit was biologically potent by confirming its previously reported function in midline crossing of RGC axons. At 48 hpf, when the earliest RGC axons just reach the anterior tectal boundary, Slit2 OE caused follower RGC axons to re-cross the midline at the forebrain/midbrain boundary (Suppl. Fig. S1C).

When Slit2 was overexpressed at 79 hpf, a stage at which RGC axons have innervated the entire tectum, we no longer observed midline crossing defects. Instead, RGC axons were seen to aberrantly project into the layers of the tectal neuropil at 6 dpf (Fig. 2M, N), including the normally non-retinorecipient lamina below the SFGS (summarized in Fig. 2O). In control RGCs, sparsely labeled by *BGUG*, heat shock had no effect on axonal laminar targeting (Fig. 2P). However, in all Slit2-OE fish examined (*n*=12), single RGC axons were shifted to deeper layers (Fig. 2Q, R). Moreover, the side profiles of Slit2-OE axons were

more than three times thicker than controls, very similar to *ast*^{ti272z} mutants and *slit1a* MOs (Fig. 2T). We conclude that Slit provides an instructive signal that guides RGC axons to their target layer in the tectum.

Robo2 acts within RGCs while Slit1a acts in tectal cells (and some RGCs)

We asked whether Robo2 and Slit1a regulate laminar RGC axon targeting cell-autonomously. Cells from *Pou4f3:mGFP* transgenic fish were transplanted into non-transgenic hosts to generate clones of one to five labeled RGCs. WT RGCs transplanted into a WT host were targeted correctly to single layers (*n*=7; Fig. 3A, B), as were axons from WT RGCs, transplanted into *ast*^{ti272z} mutant hosts (*n*=8; Fig. 3C). Mutant *ast*^{ti272z} RGCs transplanted into WT hosts exhibited mistargeting similar to that observed in *ast*^{ti272z} mutants (*n*=5; Fig 3D). Combined, these findings suggest that the Robo2 receptor acts within individual axons guiding them to their correct layer.

The *slit1a* mRNA is expressed by tectal cells and a subpopulation of RGCs (Suppl. Fig. S2). WT RGCs transplanted into a *slit1a* MO-injected host showed laminar-targeting defects similar to global *slit1a* knockdown (*n*=17; Fig. 3E). Targeting defects were more severe in anterior tectum, which is innervated earlier, presumably when MO knockdown is more complete than at later stages. Single RGCs, injected with *slit1a* MOs and transplanted into WT hosts, showed a mild but significant increase in retinal arbor thickness (13 +/− 0.4 μm, *n*=6 *slit1a*-MO, vs. 7.5 +/− 0.6 μm SEM, *n*=6 WT; $p<0.001$) (Fig. 3F). These results indicate that Slit1a acts primarily in the tectum to ensure proper targeting, but that it also contributes within some RGCs to the laminar confinement of axon arbors.

Slit interacts with Dragnet/Collagen IV both genetically and biochemically

The *drg* gene encodes Col4a5, a type IV Collagen that is secreted by skin cells overlaying the surface of the tectum. In *drg*^{s510}, the basement membrane is disrupted (Suppl. Fig. S3A). In all mutant animals examined (*n=32*), at least some axons made laminar targeting errors, as shown previously (Xiao and Baier, 2007). The similarity of targeting defects in *drg*^{s510} and Slit/Robo loss-of-function, raised the possibility that Slit interacts with type IV Collagen. We first tested whether *robo2* and *drg* interact genetically. Heterozygous *ast*^{ti272z} carriers are largely normal in RGC axon laminar-targeting (Fig. 4A). Axons that trespassed between SO and SFGS could be detected in 8% of *ast*$^{ti272Z/+}$ fish larvae imaged. This fraction was much larger in larvae doubly heterozygous for *ast*^{ti272z} and *drg*^{s510}. Here 64% (16 of 25) displayed laminar targeting defects (Fig. 4B; summarized in Fig. 4C). This genetic interaction suggested that Robo/Slit and Col4a5 might co-operate in the same signaling pathway.

To determine if Slit1 directly binds to Collagen IV, we performed solid-phase ELISA binding assays. We also included the HSPG Agrin in this analysis. Agrin is localized to the surface of the zebrafish larval tectum and is dispersed in *drg*^{s510} mutants, following the pattern observed previously with a pan-HSPG antibody (Xiao and Baier, 2007). HSPGs have been shown to bind Slit proteins (Hu, 2001) and may function as co-receptors for Slit (Johnson et al., 2004; Steigemann et al., 2004). Pairwise analysis showed that each of these three factors directly bound any of the other two (*n*=3 independent experiments, each carried out in duplicate) (Fig. 4D, E). The data also revealed that Collagen IV's binding of Agrin and Slit1 was resistant to heparin, whereas Agrin's binding of Slit1 was not (Fig. 4F). Pre-treatment of Agrin with nitrous acid to chemically degrade HS-GAG chains abolished binding to Slit1, while binding of Collagen IV was intact (data not shown). We conclude from these data that Agrin binds Slit1 via its HS-GAG chains and binds Collagen IV via its proteoglycan core. We quantified the affinity of Collagen IV binding to Slit1 with surface plasmon resonance. Slit1 was immobilized on a Biacore sensor chip and increasing amounts

of Collagen IV were added. These data confirm dose-dependent binding of the two factors with a K_D= 0.65 nM (Fig. 4G). In conclusion, *in vitro* binding assays suggest that Slit may form complexes with ECM components of the basement membrane.

Tectal neuron dendritic targeting requires Slit/Robo signaling and an intact basement membrane

We asked whether Slit/Robo signals guides the proper stratification of tectal dendrites. First, we showed that *robo2* mRNA is expressed strongly in the tectum (Fig. 5A). To confirm that the *robo2* expression is in tectal neurons (as opposed to glia or other cell types), we performed *robo2 in situ* hybridization in *Dlx5/6:GFP* transgenic fish (see Fig. 1A–C). We found that *Dlx5/6:GFP* expressing neurons also expressed *robo2* mRNA (Fig. 5B). Next we investigated Parvalbumin-positive dendrites, which are segregated into four neuropil laminae (Fig. 5C). In ast^{ti272z} mutants, parvalbumin-positive cell bodies are present in normal number and position, but their neurites appear diffuse and lamination is not detectable (Fig. 5D). In WT, the $SFGS_F$ sublamina (labeled by *pou4f3:mGFP*) precisely abuts the third lamina of parvalbumin-positive neurites (Fig. 5E). In ast^{ti272z} mutants, those same neurites greatly overlap with the RGC axons (Fig. 5F).

To label identified tectal neurons in a mosaic fashion, we generated a construct, *pDlx5/6s:Gal4*, using the previously described *Dlx5/6* promoter with a short intergenic enhancer region of the *Dlx5/6* gene. Transient expression of *Dlx5/6s:Gal4* and *UAS:Dsred* labels three cell types (Robles et al., 2001), including a bistratified type that is characterized by a single dendritic arbor in $SFGS_B$ and an axon arbor in a deeper layer (Fig. 5G). Bistratified neurons with this morphology are common in WT (40% of all labeled neurons; n=92), but entirely absent from ast^{ti272z} mutants. Instead, all of the *Dlx5/6s:Gal4* and *UAS:DsRed*-labeled neurons imaged by us (n=23) showed diffuse, nonstratified projections (Fig. 5H). While we cannot exclude that ast^{ti272z} mutants retain other stratified neuron types that escaped our sampling method, these numbers represent a significant difference between the expected and measured fractions (p<0.001).

To test the role of Col4a5 and basement membrane integrity in dendrite stratification, we imaged *Dlx5/6:GFP* tectal neurons in WT and drg^{s510} larvae. First, we looked at overall tectal neurite lamination in *Dlx5/6:GFP* transgenic fish. While six neurite layers can be identified in the WT tectum, the superficial layers in drg^{s510} mutants are often more diffuse. Bundled processes extend between the layers, which co-localize with RGC axons trespassing the SO and SFGS (Suppl. Fig. S3B). In drg^{s510} mutants, 33% (7 of 21) of the individually labeled tectal neurons with *Dlx5/6s:Gal4* and *UAS:Dsred* projected a laminated arbor with a different, novel shape — two arborizations, in SFGS and deeper neuropil, and an additional “plume” in SO (Fig. 5I). No other imaged neurons in drg^{s510} had a stratified projection pattern. This suggests that the shape of the bistratified type has been altered by the drg^{s510} mutation.

Radial glial endfeet attachment requires Dragnet, but not Slit/Robo or heparan sulfate chains

Radial glia extend their processes through the neuropil to the surface of the tectum. We asked if Slit/Robo signaling is required for proper orientation of radial glia perpendicular to the neurite layers and the attachment of their endfeet. Radial glia are labeled in the enhancer-trap lines *Gal4s1082t*, *Gal4s1061t*, and *Gal4s1013t* (Scott and Baier, 2009; Scott et al., 2007). The latter line, *Gal4s1013t*, also marks most tectal neurons in young larvae. We observed that cells with the `bottlebrush' morphology of radial glia appeared as early as 3 dpf in the zebrafish tectum (Fig. 5J). Their prominent endfeet are positioned within the basement membrane right below the tectal surface (Xiao and Baier, 2007). In ast^{ti272z}

mutants, *BGUG*-labeled radial glia appeared morphologically indistinguishable from WT (Fig. 5K). In contrast, labeled cells in the *drg*^{s510} mutants, although still discernible as radial glia, failed to develop endfeet structure at all stages examined, up until 8 dpf (Fig. 5L). Thus, an intact basement membrane is required for the differentiation of radial glia, while Slit/Robo signaling is dispensable.

We previously showed that Collagen IV binds HSPGs, which in turn provide instructive cues for RGC axon laminar targeting (Xiao and Baier, 2007). Two mutants with disrupted heparan sulfate chain synthesis, *boxer* (*box*^{tm70g}) and *dackel* (*dak*^{t0273b}) (Lee et al., 2004) display highly penetrant lamination defects similar to *drg* (*n*=18 of 18 mutants each). HSPG2 appears to be required for the radial glia attachment to the pial basement membrane in mouse (Haubst et al., 2006). We therefore considered the possibility that mislocalization of HSPGs in *drg*^{s510} mutants contributed to the detachment of radial glial endfeet. To test this idea, *Gal4s1082t* and *UAS:Kaede* transgenes were crossed into the *box*^{tm70g} mutant background. We find that endfeet attachment to the pial surface was unperturbed in *box*^{tm70g} mutants (Suppl. Fig. S3), suggesting that the heparan sulfate chains of HSPGs do not critically support these processes.

Overexpressed Slit protein accumulates in the tectal basement membrane

Slit binds both HSPGs and Collagen IV *in vitro*, suggesting that Slit protein might be present at higher concentration on the surface of the tectum. Testing this prediction is not straightforward, as there is no antibody available for Slit1 immunohistochemistry. We therefore used the *hsp70l:Slit2-GFP* transgenic line (Yeo et al., 2001) to misexpress a Slit2-GFP fusion protein in vivo. We reasoned that the spatial distribution of the Slit2-GFP fluorescent signal would approximate the tissue localization of endogenous Slits, since their biochemical binding affinities are likely to be highly similar. A *hsp70l:Slit2-GFP* transgenic fish was crossed to a *Gal4s1013t* and *UAS:mmCherry* double transgenic carrier (Arrenberg et al., 2009). In these fish, the entire neuropil is labeled with membrane-targeted mCherry. To rule out a spatial bias of heatshock induction, we first examined the GFP signal distribution in *hsp70l:Gal4; UAS:GFP* fish. GFP intensity in *hsp70l:Gal4;UAS:GFP* fish tectum did not show local enrichment following heat-shock treatment (Suppl. Fig. S4). Furthermore, RNA in situ hybridization did not show preferential transcription of *slit2-gfp* mRNA near the surface or in specific subsets of cells (data not shown).

We found that, three hours after heat-shock induction, the fluorescence signal from Slit2-GFP protein concentration is three times brighter at the surface than the rest of the tectal neuropil (Fig. 6A–C). At 12 hours post-induction, a thin layer above the SO is brightly fluorescent, while the GFP signal has become undetectable in the neuropil (Fig. 6D, E; summarized in Fig. 6F). In striking contrast to WT (Fig. 6G, J), *drg*^{s510} mutants showed no Slit2-GFP accumulation at the surface of the tectum. Instead, we observed brightly fluorescent puncta in the middle of the neuropil (Fig. 6H, K). Slit2-GFP surface accumulation is still evident in *dak*^{t0273b} mutants crossed to *hsp70l:slit2-GFP* (Fig. 6I, L). Interestingly, the GFP signal intensity appeared to remain high in the neuropil of *dak*^{t0273b} mutants when compared to WT. This might indicate that HSPGs play a role in Slit protein degradation or translocation. Together, our results indicate that Collagen IV, but not HSPGs, are required for the surface localization of Slit protein in the tectum.

Slit surface localization is dependent on the integrity of the radial glia

We asked if radial glial endfeet might play a role in Slit localization by imaging glia together with Slit2-GFP. The glia driver line *Gal4s1082t* was crossed to *UAS:Kaede*. Kaede protein was then photoconverted with ultraviolet light from green to red. In WT, glial endfeet were decorated with Slit2-GFP (Fig. 7A; Suppl Fig. S5). In *drg*^{s510} mutants, in

which endfeet fail to form, we observed abnormal puncta of Slit2-GFP deep in the neuropil, which were not co-localized with the distal ends of radial glial cells (Fig. 7B). This spatial correlation suggested that proper endfeet positioning contributes to surface localization of Slit.

To test if radial glia are required for localization of Slit, we ablated radial glia in the *hsp70l:Slit2-GFP* tectum. Enhancer trap line *Gal4s1061t* was crossed to *UAS:nfsb-mCherry* (Davison et al., 2007) to express nitroreductase in radial glia. When treated with the prodrug metronidazole (MTZ), nitroreductase catalyzes the production of a cytotoxic product, which induces cell death. In untreated, heat-shocked fish, we observed co-localization of Slit2-GFP with the glial end feet, as before (Fig. 7C, C'). However, in MTZ-treated fish, in which radial glia had been eliminated at 60 hpf, the Slit2-GFP band was greatly diminished (Fig. 7 D, D'). Conversely, surface attachment of radial glial endfeet was normal ast^{ti272z} mutants (data not shown). We conclude from these experiments that the integrity of the radial glia is essential for Slit localization, while Slit is not necessary for glial endfeet anchoring.

Discussion

Wiring up hundreds of cell types in a specific fashion presents a formidable challenge to the developing nervous system. Cell-cell recognition, through transmembrane glycoproteins of the cadherin, immunoglobulin, and semaphorin superfamilies, results in selective adhesion or repulsion of axons and dendrites (Inoue and Sanes, 1997; Matsuoka et al., 2010; Sanes and Yamagata, 2009; Yamagata and Sanes, 1995a; Yamagata and Sanes, 1995b). However, cell-surface interactions are insufficient to account for the reproducible order of neuronal connections. Our studies have now added a new class of mechanism by showing that the layered architecture of the retinotectal neuropil is organized by the secreted axon guidance molecule Slit, which is in turn stabilized by Collagen IV in the basement membrane at the surface of the tectum.

Collagen IV appears to organize a complex macromolecular and cellular scaffold at the surface of the tectum, which consists of radial glial endfeet and secreted factors, such as Slit and HSPGs. Each of them contributes to lamina-specific targeting of RGC axons, either directly or in an accessory role. A similar organizer function for Collagen IV has been shown in dorsal-ventral patterning of the *Drosophila* embryo, where it stabilizes a spatial gradient of the morphogen Decapentaplegic (Wang et al., 2008). Similarly, Collagen IV-bound Netrin has been reported to act as a local guidance cue for adhesion and tissue morphogenesis (Yebra et al., 2003). It is possible that Collagen IV serves as a multipurpose substrate for the presentation of extracellular cues in a wide range of developmental contexts.

Slit has been shown to guide commissural axons away from the midline of the vertebrate spinal cord and the *Drosophila* nerve cord (Rajagopalan et al., 2000; Simpson et al., 2000). After crossing the midline, lateral positions of the commissural tracts depend on the total number of Robo copies expressed in the axons, while the specific isoform complement (Robo, Robo2, or Robo3) does not seem to matter (Spitzweck et al., 2010). Mathematical models predict that the Slit gradient at the midline should be stabilized by the substrate, rather than sustained by free diffusion from the midline source (Goodhill, 2003). However, direct evidence for a spatial gradient in this system is missing. Our findings in the zebrafish retinotectal system raise the possibility that type IV Collagen may serve to anchor a Slit gradient at the spinal cord midline as well.

In the tectum, Slit seems to have either repulsive or attractive functions, depending on the subpopulation of neurites. Axons projecting to the SFGS are normally repelled by Slit,

resulting in their misrouting to the surface in *ast* mutants. In contrast, a substantial proportion of axons, from among those projecting to the SO, appear to be unaffected by experimental manipulation of Slit/Robo signaling. Another subset of SO-projecting axons are deflected from the tectal surface in *ast* mutants and in *slit1a* morphants, suggesting that the high Slit concentration is attractive to some RGCs. Such a positive, axon growth-promoting function of Slit has previously been reported for various types of sensory neurons in mouse (Wang et al., 1999) and zebrafish (Yeo et al., 2004). While there are no detectable differences in *robo2* mRNA expression across the population of RGCs (Lee et al., 2001), the zebrafish *robo2* transcript has been shown to be alternatively spliced, giving rise to several isoforms, some of which are present only in certain tissues or developmental stages (Dalkic et al., 2006). In mouse spinal cord, two functionally antagonistic isoforms of Robo3 are present in the commissural neurons (Chen et al., 2008). Distinct isoforms with differential affinities toward Slit or different downstream effectors could be expressed in subtypes of axons, resulting in subtype-specific laminar choices in the tectum. Alternatively, levels of functional Robo2 could vary due to post-transcriptional regulation. For instance, the microRNA miR-218 lowers the activity of *robo1* (Tie et al., 2010). A functional screen of retina-specific microRNAs, however, has so far not yielded any that control lamina-specific targeting (T. X., unpublished data). It is also possible that the SO-projecting axon populations carry a specific co-receptor that either mutes or sign-inverts the Robo2 signal, as shown for the Netrin-receptor Unc5 in the commissural axons of the spinal cord (Hong et al., 1999). Future work will be concerned the molecular mechanism that renders RGC types differentially sensitive to Slit.

HSPGs play a role in the development of the retinotectal neuropil, as evidenced by laminar targeting defects in both *box* and *dak* mutants (Xiao and Baier, 2007; this study). These mutants are unable to synthesize heparan sulfate chains (Lee et al., 2004). Slits have been shown in other systems to bind to HSPGs, and this binding is essential for their biological activity (Hu, 2001; Hussain et al., 2006; Van Vactor et al., 2006) or their extracellular distribution (Johnson et al., 2004). In the context of retinotectal lamination, however, it is uncertain if Slit function depends on HSPGs. While the HSPG Agrin binds Slit in vitro through its heparan sulfate chains, Slit2-GFP is localized apparently normally in *dak* mutants. Collagen IV binds Agrin in vitro and localizes it in vivo to the surface of the tectum (Xiao and Baier, 2007; G. C., unpublished data). It is still possible that both Collagen IV and HSPGs act in concert to anchor Slit in the basement membrane. We conclude that HSPGs contribute to laminar targeting of axons and bind Slit in vitro, but are not required for basement-membrane localization of Slit, presumably because of redundancy with Collagen IV.

We found that radial glia contribute to the layered architecture of the tectal neuropil. Their endfeet are attached to the basement membrane by Collagen IV and are decorated with GFP fluorescence following heatshock induction of Slit2-GFP. Targeted ablation of radial glia (with nitroreductase) diminishes the Slit2-GFP band at the tectal surface and results in laminar targeting defects very similar to the phenotypes of *ast* or *drg*. In *drg* mutants, both glial endings and Slit2-GFP are displaced from the surface. Interestingly, Slit2-GFP and glial endfeet are no longer co-localized in the *drg* mutant, suggesting that their association in WT is probably not due to a physical binding of Slit to the glial endfeet. Rather the surface accumulation could be generated by directed transport of Slit, local secretion, and/or local protection from degradation near the glial endfeet, with an intact basement membrane necessary for these processes to occur.

In conclusion, our studies point to an enrichment of Slit at the surface of the nascent tectal neuropil. Slit molecules are secreted, then deposited into the ECM and stabilized by radial glial endfeet. We propose that the high concentration of Slit protein at the tectal surface

results in a signaling gradient that repels certain types of axons and dendrites and attracts other types. While we cannot reliably determine the decreasing concentration of Slit at a distance from the basement membrane due to technical limitations (lack of a specific antibody), a spatial gradient of Slit seems more consistent than a step-like boundary with our observation that Slit/Robo signaling extends into the deep layers of the tectum. The shared responsiveness of axons and dendrites to Slit brings matching synaptic partners into spatial register along the superficial-to-deep axis of the tectum. It seems likely that other secreted, ECM-bound guidance factors exist that impart lamina-specific positional information on both axons and dendrites.

Experimental Procedures

Zebrafish lines

Zebrafish (TL and WIK strains) were raised and bred according to standard procedures (see Supplementary Information). A list of mutant alleles and transgenic lines is provided in the supplement.

Heatshock induction

Heatshock induction was performed as previously described (Xiao et al., 2003). Briefly, larvae were transferred into a 50ml Falcon tube and then submerged in a 39°C water bath for 40 min.

Design and injection of morpholinos and DNA constructs

Morpholino knockdown analysis was performed according to standard procedures. Sequences and other details are given in the Supplement.

Immunohistochemistry and RNA in situ hybridization

Stainings were performed according to published procedures (see Supplementary Information).

Cell transplantation

Cell transplantation was performed as described before (Xiao and Baier, 2007). Donors were labeled with Rodamine Alexa 555 (Molecular Probes) at 1–4 cell stage. 3–5 cells were transplanted from donors to dorsal region of hosts at germ ring to shield stage. Only hosts with no donor clones in the brain were imaged.

Protein binding assays

Either recombinant mouse Slit1 (0.5 μg) or Agrin immunopurified from chick vitreous (0.5 μg) was immobilized to wells of ELISA plates, and binding of the target protein (i.e., Col IV) was quantified using antibody to the target protein, biotinylated secondary antibody, and Vectastain ABC kits. For surface plasmon resonance, Slit1 was immobilized on a Biacore sensor chip and increasing amounts of Col IV were exposed to Slit1. Sensograms were corrected by subtraction of BSA background binding. Additional details in Supplement.

Cell ablation with nitroreductase

Cell ablations were performed following a previously described protocol (Curado et al., 2008). Zebrafish larvae were incubated in 10 mM metronidazole, 0.1% DMSO, in E3 buffer for 6 hours and then washed 5× in E3.

In vivo imaging and quantification

Preparation of live larvae, confocal microscopy, and three-dimensional reconstruction of individual neurons were performed as described (Xiao and Baier, 2007). Images were analyzed with ImageJ and Volocity.

Supplementary Material

Refer to Web version on PubMed Central for supplementary material.

Acknowledgments

We thank Hitoshi Okamoto, Marc Ekker, Chi-Bin Chien and members of our laboratory for reagents and fish lines. This work was funded by NIH R01 EY013855 and EY012406.

References

Arrenberg AB, Del Bene F, Baier H. Optical control of zebrafish behavior with halorhodopsin. Proc Natl Acad Sci U S A. 2009; 106:17968–73. [PubMed: 19805086]

Baier H, Klostermann S, Trowe T, Karlstrom RO, Nusslein-Volhard C, Bonhoeffer F. Genetic dissection of the retinotectal projection. Development. 1996; 123:415–25. [PubMed: 9007259]

Brose K, Bland KS, Wang KH, Arnott D, Henzel W, Goodman CS, Tessier-Lavigne M, Kidd T. Slit proteins bind Robo receptors and have an evolutionarily conserved role in repulsive axon guidance. Cell. 1999; 96:795–806. [PubMed: 10102268]

Campbell DS, Stringham SA, Timm A, Xiao T, Law MY, Baier H, Nonet ML, Chien CB. Slit1a inhibits retinal ganglion cell arborization and synaptogenesis via Robo2-dependent and -independent pathways. Neuron. 2007; 55:231–45. [PubMed: 17640525]

Chen Z, Gore BB, Long H, Ma L, Tessier-Lavigne M. Alternative splicing of the Robo3 axon guidance receptor governs the midline switch from attraction to repulsion. Neuron. 2008; 58:325–32. [PubMed: 18466743]

Curado S, Stainier DY, Anderson RM. Nitroreductase-mediated cell/tissue ablation in zebrafish: a spatially and temporally controlled ablation method with applications in developmental and regeneration studies. Nat Protoc. 2008; 3:948–54. [PubMed: 18536643]

Dalkic E, Kuscu C, Sucularli C, Aydin IT, Akcali KC, Konu O. Alternatively spliced Robo2 isoforms in zebrafish and rat. Dev Genes Evol. 2006; 216:555–63. [PubMed: 16625395]

Davison JM, Akitake CM, Goll MG, Rhee JM, Gosse N, Baier H, Halpern ME, Leach SD, Parsons MJ. Transactivation from Gal4-VP16 transgenic insertions for tissue-specific cell labeling and ablation in zebrafish. Dev Biol. 2007; 304:811–24. [PubMed: 17335798]

Erskine L, Williams SE, Brose K, Kidd T, Rachel RA, Goodman CS, Tessier-Lavigne M, Mason CA. Retinal ganglion cell axon guidance in the mouse optic chiasm: expression and function of robos and slits. J Neurosci. 2000; 20:4975–82. [PubMed: 10864955]

Fricke C, Lee JS, Geiger-Rudolph S, Bonhoeffer F, Chien CB. astray, a zebrafish roundabout homolog required for retinal axon guidance. Science. 2001; 292:507–10. [PubMed: 11313496]

Ghanem N, Jarinova O, Amores A, Long Q, Hatch G, Park BK, Rubenstein JL, Ekker M. Regulatory roles of conserved intergenic domains in vertebrate Dlx bigene clusters. Genome Res. 2003; 13:533–43. [PubMed: 12670995]

Goodhill GJ. A theoretical model of axon guidance by the Robo code. Neural Comput. 2003; 15:549–64. [PubMed: 12625331]

Gosse NJ, Nevin LM, Baier H. Retinotopic order in the absence of axon competition. Nature. 2008; 452:892–5. [PubMed: 18368050]

Halfter W, Dong S, Yip YP, Willem M, Mayer U. A critical function of the pial basement membrane in cortical histogenesis. J Neurosci. 2002; 22:6029–40. [PubMed: 12122064]

Halfter W, Schurer B. Disruption of the pial basal lamina during early avian embryonic development inhibits histogenesis and axonal pathfinding in the optic tectum. J Comp Neurol. 1998; 397:105–17. [PubMed: 9671282]

Haubst N, Georges-Labouesse E, De Arcangelis A, Mayer U, Gotz M. Basement membrane attachment is dispensable for radial glial cell fate and for proliferation, but affects positioning of neuronal subtypes. Development. 2006; 133:3245–54. [PubMed: 16873583]

Hong K, Hinck L, Nishiyama M, Poo MM, Tessier-Lavigne M, Stein E. A ligand-gated association between cytoplasmic domains of UNC5 and DCC family receptors converts netrin-induced growth cone attraction to repulsion. Cell. 1999; 97:927–41. [PubMed: 10399920]

Hu H. Cell-surface heparan sulfate is involved in the repulsive guidance activities of Slit2 protein. Nat Neurosci. 2001; 4:695–701. [PubMed: 11426225]

Huberman AD, Clandinin TR, Baier H. Molecular and cellular mechanisms of lamina-specific axon targeting. Cold Spring Harb Perspect Biol. 2010; 2:a001743. [PubMed: 20300211]

Huberman AD, Manu M, Koch SM, Susman MW, Lutz AB, Ullian EM, Baccus SA, Barres BA. Architecture and activity-mediated refinement of axonal projections from a mosaic of genetically identified retinal ganglion cells. Neuron. 2008; 59:425–38. [PubMed: 18701068]

Huberman AD, Wei W, Elstrott J, Stafford BK, Feller MB, Barres BA. Genetic identification of an On-Off direction-selective retinal ganglion cell subtype reveals a layer-specific subcortical map of posterior motion. Neuron. 2009; 62:327–34. [PubMed: 19447089]

Hussain SA, Piper M, Fukuhara N, Strochlic L, Cho G, Howitt JA, Ahmed Y, Powell AK, Turnbull JE, Holt CE, et al. A molecular mechanism for the heparan sulfate dependence of slit-robo signaling. J Biol Chem. 2006; 281:39693–8. [PubMed: 17062560]

Hutson LD, Chien CB. Pathfinding and error correction by retinal axons: the role of astray/robo2. Neuron. 2002; 33:205–17. [PubMed: 11804569]

Inoue A, Sanes JR. Lamina-specific connectivity in the brain: regulation by N-cadherin, neurotrophins, and glycoconjugates. Science. 1997; 276:1428–31. [PubMed: 9162013]

Johnson KG, Ghose A, Epstein E, Lincecum J, O'Connor MB, Van Vactor D. Axonal heparan sulfate proteoglycans regulate the distribution and efficiency of the repellent slit during midline axon guidance. Curr Biol. 2004; 14:499–504. [PubMed: 15043815]

Kay JN, Finger-Baier KC, Roeser T, Staub W, Baier H. Retinal ganglion cell genesis requires lakritz, a Zebrafish atonal Homolog. Neuron. 2001; 30:725–36. [PubMed: 11430806]

Kay JN, Link BA, Baier H. Staggered cell-intrinsic timing of ath5 expression underlies the wave of ganglion cell neurogenesis in the zebrafish retina. Development. 2005; 132:2573–85. [PubMed: 15857917]

Kidd T, Bland KS, Goodman CS. Slit is the midline repellent for the robo receptor in Drosophila. Cell. 1999; 96:785–94. [PubMed: 10102267]

Lee JS, Ray R, Chien CB. Cloning and expression of three zebrafish roundabout homologs suggest roles in axon guidance and cell migration. Dev Dyn. 2001; 221:216–30. [PubMed: 11376489]

Lee JS, von der Hardt S, Rusch MA, Stringer SE, Stickney HL, Talbot WS, Geisler R, Nusslein-Volhard C, Selleck SB, Chien CB, et al. Axon sorting in the optic tract requires HSPG synthesis by ext2 (dackel) and extl3 (boxer). Neuron. 2004; 44:947–60. [PubMed: 15603738]

Lemke G, Reber M. Retinotectal mapping: new insights from molecular genetics. Annu Rev Cell Dev Biol. 2005; 21:551–80. [PubMed: 16212507]

Li HS, Chen JH, Wu W, Fagaly T, Zhou L, Yuan W, Dupuis S, Jiang ZH, Nash W, Gick C, et al. Vertebrate slit, a secreted ligand for the transmembrane protein roundabout, is a repellent for olfactory bulb axons. Cell. 1999; 96:807–18. [PubMed: 10102269]

Matsuoka RL, Nguyen-Ba-Charvet KT, Parray A, Badea TC, Chedotal A, Kolodkin AL. Transmembrane semaphorin signalling controls laminar stratification in the mammalian retina. Nature. 2010; 470:259–63. [PubMed: 21270798]

May PJ. The mammalian superior colliculus: laminar structure and connections. Prog Brain Res. 2006; 151:321–78. [PubMed: 16221594]

Nevin LM, Robles E, Baier H, Scott EK. Focusing on optic tectum circuitry through the lens of genetics. BMC Biol. 2010; 8:126. [PubMed: 20920150]

Nevin LM, Taylor MR, Baier H. Hardwiring of fine synaptic layers in the zebrafish visual pathway. Neural Dev. 2008; 3:36. [PubMed: 19087349]

Nevin LM, Xiao T, Staub W, Baier H. Topoisomerase IIß is required for lamina-specific targeting of retinal ganglion cell axons and dendrites. Development. 2011; 138:2457–2465. [PubMed: 21610027]

Plump AS, Erskine L, Sabatier C, Brose K, Epstein CJ, Goodman CS, Mason CA, Tessier-Lavigne M. Slit1 and Slit2 cooperate to prevent premature midline crossing of retinal axons in the mouse visual system. Neuron. 2002; 33:219–32. [PubMed: 11804570]

Poggi L, Vitorino M, Masai I, Harris WA. Influences on neural lineage and mode of division in the zebrafish retina in vivo. J Cell Biol. 2005; 171:991–9. [PubMed: 16365165]

Rajagopalan S, Vivancos V, Nicolas E, Dickson BJ. Selecting a longitudinal pathway: Robo receptors specify the lateral position of axons in the Drosophila CNS. Cell. 2000; 103:1033–45. [PubMed: 11163180]

Rakic P. Elusive radial glial cells: historical and evolutionary perspective. Glia. 2003; 43:19–32. [PubMed: 12761862]

Robles E, Smith SJ, Baier H. Characterization of genetically targeted neuron types in the zebrafish optic tectum. Front Neural Circuits. 2011; 5:1. [PubMed: 21390291]

Sanes JR, Yamagata M. Many paths to synaptic specificity. Annu Rev Cell Dev Biol. 2009; 25:161–95. [PubMed: 19575668]

Scott EK, Baier H. The cellular architecture of the larval zebrafish tectum, as revealed by gal4 enhancer trap lines. Front Neural Circuits. 2009; 3:13. [PubMed: 19862330]

Scott EK, Mason L, Arrenberg AB, Ziv L, Gosse NJ, Xiao T, Chi NC, Asakawa K, Kawakami K, Baier H. Targeting neural circuitry in zebrafish using GAL4 enhancer trapping. Nat Methods. 2007; 4:323–6. [PubMed: 17369834]

Simpson JH, Bland KS, Fetter RD, Goodman CS. Short-range and long-range guidance by Slit and its Robo receptors: a combinatorial code of Robo receptors controls lateral position. Cell. 2000; 103:1019–32. [PubMed: 11163179]

Spitzweck B, Brankatschk M, Dickson BJ. Distinct protein domains and expression patterns confer divergent axon guidance functions for Drosophila Robo receptors. Cell. 2010; 140:409–20. [PubMed: 20144763]

Steigemann P, Molitor A, Fellert S, Jackle H, Vorbruggen G. Heparan sulfate proteoglycan syndecan promotes axonal and myotube guidance by slit/robo signaling. Curr Biol. 2004; 14:225–30. [PubMed: 14761655]

Tie J, Pan Y, Zhao L, Wu K, Liu J, Sun S, Guo X, Wang B, Gang Y, Zhang Y, et al. MiR-218 inhibits invasion and metastasis of gastric cancer by targeting the Robo1 receptor. PLoS Genet. 2010; 6:e1000879. [PubMed: 20300657]

Van Vactor D, Wall DP, Johnson KG. Heparan sulfate proteoglycans and the emergence of neuronal connectivity. Curr Opin Neurobiol. 2006; 16:40–51. [PubMed: 16417999]

Wang KH, Brose K, Arnott D, Kidd T, Goodman CS, Henzel W, Tessier-Lavigne M. Biochemical purification of a mammalian slit protein as a positive regulator of sensory axon elongation and branching. Cell. 1999; 96:771–84. [PubMed: 10102266]

Wang X, Harris RE, Bayston LJ, Ashe HL. Type IV collagens regulate BMP signalling in Drosophila. Nature. 2008; 455:72–7. [PubMed: 18701888]

Xiao T, Baier H. Lamina-specific axonal projections in the zebrafish tectum require the type IV collagen Dragnet. Nat Neurosci. 2007; 10:1529–37. [PubMed: 17982451]

Xiao T, Roeser T, Staub W, Baier H. A GFP-based genetic screen reveals mutations that disrupt the architecture of the zebrafish retinotectal projection. Development. 2005; 132:2955–67. [PubMed: 15930106]

Xiao T, Shoji W, Zhou W, Su F, Kuwada JY. Transmembrane sema4E guides branchiomotor axons to their targets in zebrafish. J Neurosci. 2003; 23:4190–8. [PubMed: 12764107]

Yamagata M, Sanes JR. Lamina-specific cues guide outgrowth and arborization of retinal axons in the optic tectum. Development. 1995a; 121:189–200. [PubMed: 7867499]

Yamagata M, Sanes JR. Target-independent diversification and target-specific projection of chemically defined retinal ganglion cell subsets. Development. 1995b; 121:3763–76. [PubMed: 8582286]

Yebra M, Montgomery AM, Diaferia GR, Kaido T, Silletti S, Perez B, Just ML, Hildbrand S, Hurford R, Florkiewicz E, et al. Recognition of the neural chemoattractant Netrin-1 by integrins alpha6beta4 and alpha3beta1 regulates epithelial cell adhesion and migration. Dev Cell. 2003; 5:695–707. [PubMed: 14602071]

Yeo SY, Little MH, Yamada T, Miyashita T, Halloran MC, Kuwada JY, Huh TL, Okamoto H. Overexpression of a slit homologue impairs convergent extension of the mesoderm and causes cyclopia in embryonic zebrafish. Dev Biol. 2001; 230:1–17. [PubMed: 11161558]

Yeo SY, Miyashita T, Fricke C, Little MH, Yamada T, Kuwada JY, Huh TL, Chien CB, Okamoto H. Involvement of Islet-2 in the Slit signaling for axonal branching and defasciculation of the sensory neurons in embryonic zebrafish. Mech Dev. 2004; 121:315–24. [PubMed: 15110042]

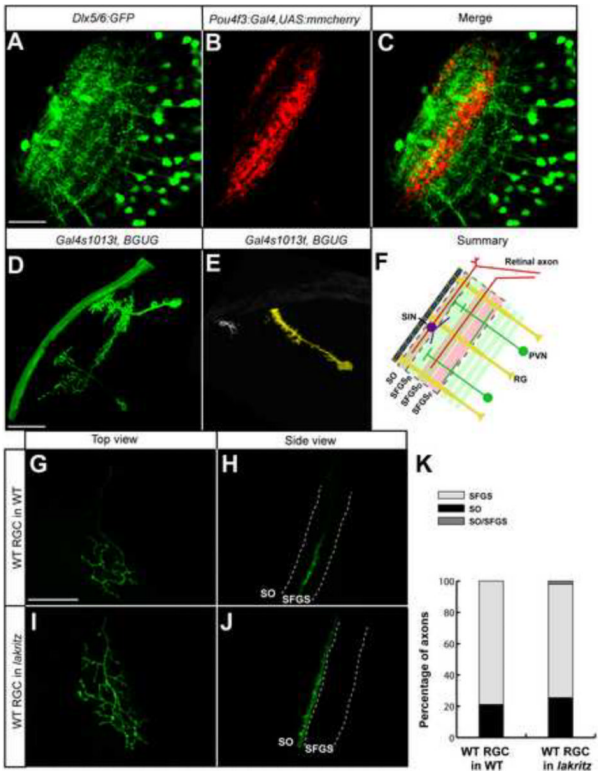

Figure 1. Axons, dendrites and radial glia contribute to the laminar architecture of the zebrafish tectum

Images were taken at 6 dpf and are merged confocal z-stacks (projections). **A**. *Dlx5/6:GFP*-labeled tectal neuron. **B**. *Pou4f3:Gal4* and *UAS:mmCherry* labeled RGC axon. **C.** Merged image of A and B. **D.** Tectal neurons, sparsely labeled with *Gal4s1013t* and *BGUG*. **E.** Radial glial cell and a superficial tectal neuron, labeled in the same tectum. **F.** Schematic summary of the laminar composition of the larval tectum. Scale bars are 20 μm. **G–J**. *Pou4f3:mGFP*-positive, WT donor RGC transplanted into a non-transgenic host larva. Host was either WT (G, H) or *lak*^{th241} (I, J). G and I are top views. H and J are rotated views of the confocal image stacks in G and I to best show axonal lamination. **K.** Quantification of transplanted RGC laminar choices. Single axons behave very similarly in crowded (transplanted into WT) vs. RGC-depleted (transplanted into *lak*^{th241}) conditions.

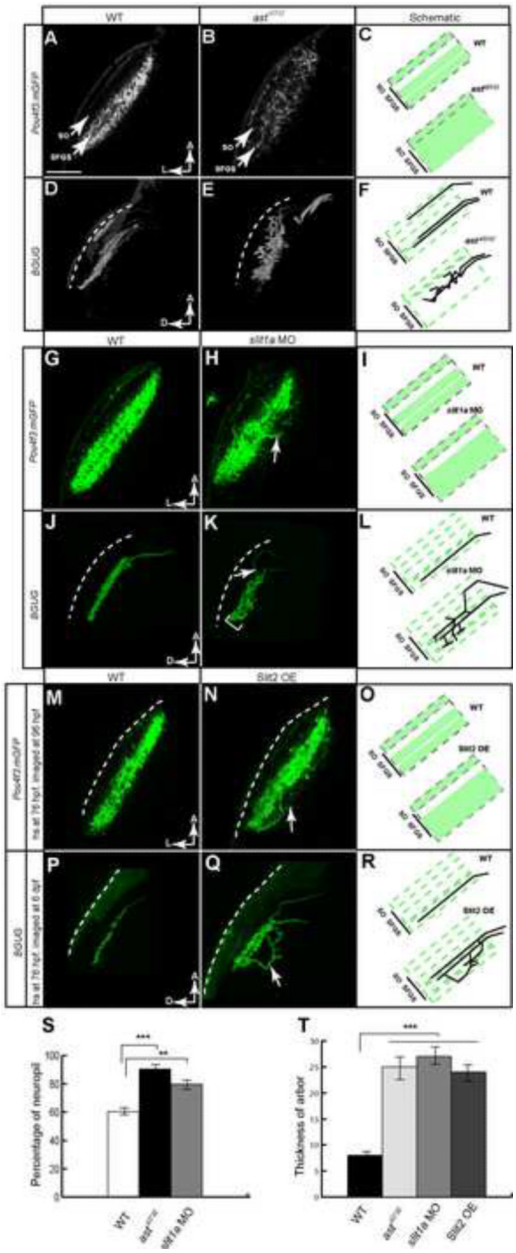

Figure 2. Robo/Slit signaling is required for RGC axon laminar targeting

A–C. Single optical sections of the tectum in *Pou4f3:mGFP* transgenic larvae at 6 dpf. RGC axons (labeled with membrane-targeted GFP) remain in their target lamina in WT (A) and cross the laminar boundaries in the *ast*^{ti272z} mutant. C is a schematic summary. **D–F**. Projections of confocal images of the WT (D) and *ast*^{ti272z} (E) tectum in *BGUG* transgenic larva at 6 dpf. Image stacks were rotated to best show laminae. Arrows point at the axons leaving their target layer. Dashed lines indicate the skin overlaying the tectum. F is a schematic summary. **G–I**. Single optical sections of the tectum in *Pou4f3:mGFP* transgenic larvae at 5 dpf. G is a control fish. H is a *slit1a* morphant. I is a schematic summary. **J–L**. Projections of confocal images of the control (J) and *slit1a* morphant (K) tectum in BGUG transgenic larva at 5 dpf. L is a schematic summary. **M–O**. Single optical sections of the tectum in *Pou4f3:mGFP* transgenic larvae. M is a control fish. N is a *hsp70l:slit2-GFP* transgenic carrier. Both were heat-shocked at 76 hpf. O is a schematic summary. **P–R**.

Projections of confocal images of the control (P) and *hsp70l:slit2-GFP* (Q) tectum in *BGUG* transgenic larva at 6 dpf. Arrows point at axons projecting deeper than SFGS. R is a schematic summary. **S**. Quantification of *Pou4f3:mGFP* RGC laminar position. **T**. Quantification of RGC arbor thickness. ***, $p<0.001$. Scale bar is 20 μm.

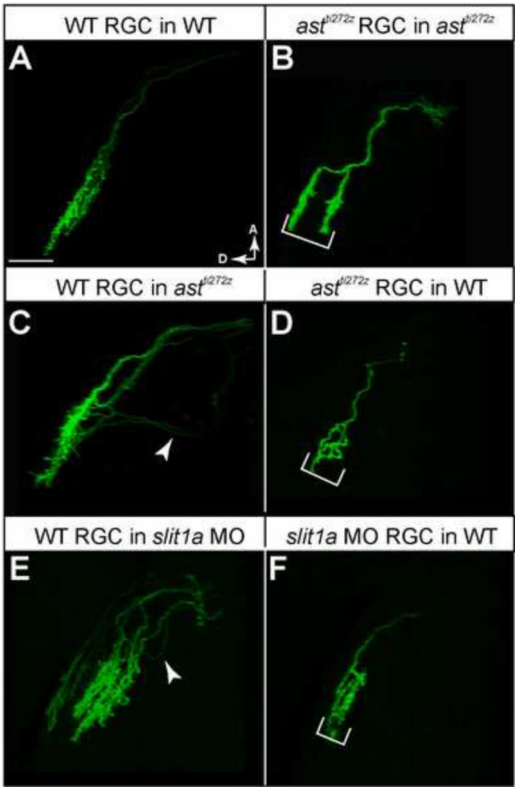

Figure 3. Robo2 acts in a retina-autonomous fashion, and Slit1 acts strongly in the tectum and weakly in the retina

Images are projections of confocal image stacks, rotated to best show laminae. Fish were 5 dpf. **A**. WT RGC transplanted into WT larva. **B** *ast*^{ti272z} RGC transplanted into *ast*^{ti272z} larva. **C**. WT RGC transplanted into *ast*^{ti272z} larva. **D**. *ast*^{ti272z} RGC transplanted into WT larva. **E**. WT RGC transplanted into *slit1a* morphant. **F**. *slit1a* morphant RGC transplanted into WT larva. Arrowheads point at mistargeted axons. Brackets indicate expanded arbor thickness. Scale bar is 20 μm.

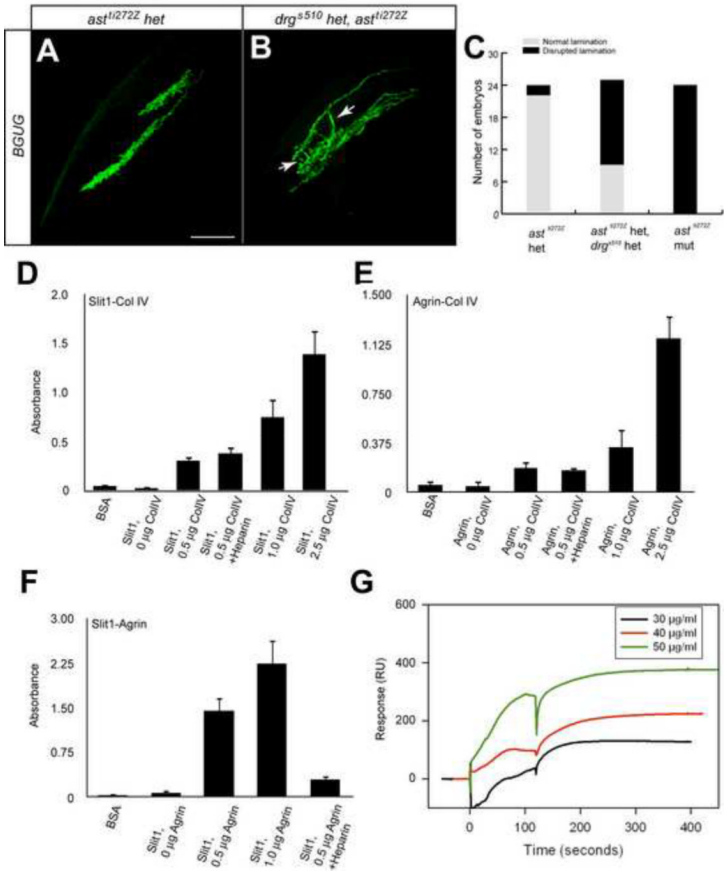

Figure 4. Collagen IV interacts genetically with, and directly binds to, Slit

A, B. Projections of confocal images of *BGUG*-labeled RGC axons in WT (A) and a double-heterozygous carrier of *drg*^{s510} and *ast*^{ti272z} at 6 dpf. Arrows point at axons that trespass the laminae. **C**. Quantification of RGC axon targeting defects. **D, E**. Analysis of Col IV, Slit1 and Agrin interactions using solid-phase ELISA binding assays (*n*=3, using duplicate samples in each experiment). Agrin and Slit1 bind Col IV via protein-protein interactions (HS-independent, not inhibited by exogenous heparin), and Agrin binds Slit1 via its HS-GAG chains (marked reduction in presence of heparin). **F**. Analysis of Col IV ligand binding to Slit1 using surface plasmon resonance. Col IV binds to Slit1 in a dose-dependent fashion, with a K_D= 0.65 nM.

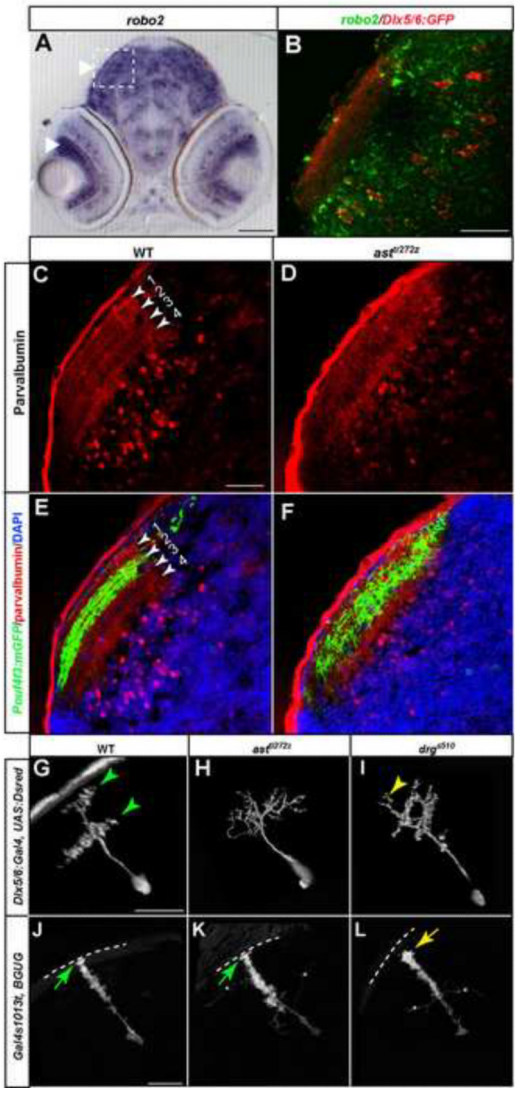

Figure 5. Tectal dendrite stratification requires both Robo/Slit signaling and Collagen IV

A. In situ hybridization, showing that *robo2* mRNA is expressed in both RGCs and tectal neurons. **B**. Double labeling of *Dlx5/6:GFP* (red) expressing tectal neurons and *robo2* mRNA (green). **C, D**. Sections of tectum labeled with anti-parvalbumin at 6 dpf. WT tectum (C) shows four distinct laminae. No lamination is detected in ast^{ti272z} tectum (D). **E, F**. Sections of WT (E) and ast^{ti272z} (F) tectum labeled with anti-parvalbuminin (red), anti-GFP (green) and DAPI (blue). Laminae are numbered in E as in C. **G–I**. Projections of confocal images of tectal neurons, transiently labeled with *Dlx5/6:Gal4* and *UAS:Dsred* at 6 dpf. In WT (G), neurites are organized into two laminae. In ast^{ti272z} (H), no lamination is detectable. In drg^{s510} (I), the two laminae are more closely spaced, and ectopic neurites extend outside the superficial layer. **J–L**. Radial glial endfeet attachment requires Col4a5. Projections of confocal images of radial glia in WT (J), ast^{ti272z} (K) and drg^{s510} (L) at 6 dpf. Arrows point at the endfeet anchored within the basement membrane. Asterisks (*) indicate processes from other cells. Scale bar is 40 μm in A. Scale bars are 20 μm in B, C, G, J.

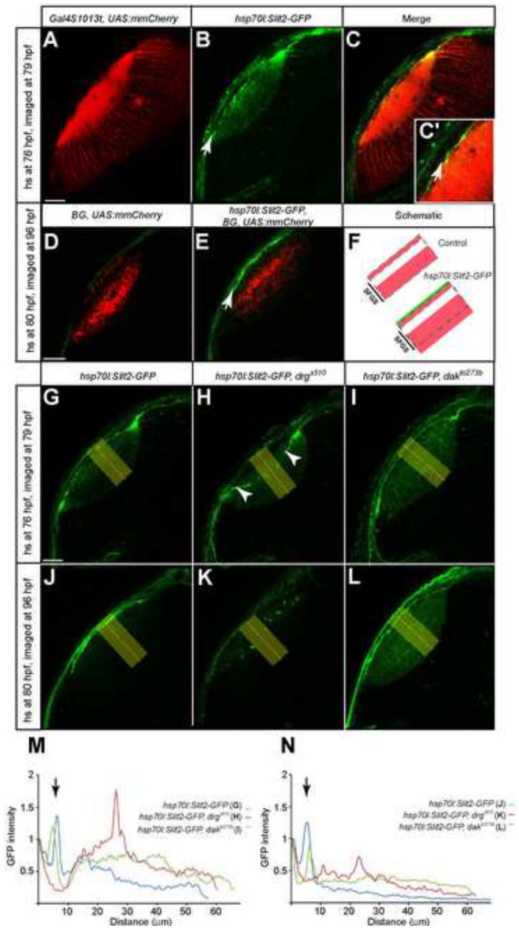

Figure 6. Slit localization in the optic tectum requires Col4a5 but not HSPGs

A–C. Optical section of a 79 hpf *hsp70l:Slit2-GFP, Gal4s1013t, UAS:mmCherry* tectum, heatshocked at 76 hpf. Many tectal neurons are labeled with mmCherry (red, A). Slit2-GFP (green, B) is enriched at the surface of the tectal neuropil (arrow). C is a merged image. **D–F**. Optical sections of 96 hpf hsp70l:Slit2-GFP, Pou4f3:Gal4 (Brn3c:Gal4, BG), UAS:mmCherry tecta, heatshocked at 80 hpf. RGC axons (red) are shown in non-heatshocked (D) and heatshocked fish (E). Arrow points at the accumulation of Slit2-GFP superficial to SO. F is a schematic summary. **G–L**. Optical sections of *hsp70l:Slit2-GFP* tecta in WT (G, J), *drg*^{s510} (H, K), and *dak*^{t0273b} (I, L). Larvae were either heatshocked at 76 hpf and imaged at 79 hpf (G–I) or heatshocked at 80 hpf and imaged at 96 hpf (J–L). **M, N**. Densitometric plots of GFP intensity in the yellow rectangle areas in panels G–L. M shows distribution 3 hours post-induction. N shows distribution 16 hours post-induction. Intensity is normalized to skin autofluorescence level (first peak at 0 μm). In WT, Slit2-GFP accumulates beneath the skin (second peak at ca. 8 μm from the surface, indicated by arrows) and is cleared from the neuropil. In *drg*^{s510}, Slit2-GFP accumulates in the neuropil, away from the surface. In *dak*^{t0273b}, Slit2-GFP is surface-localized, but remains also in the neuropil. Scale bar is 20 μm.

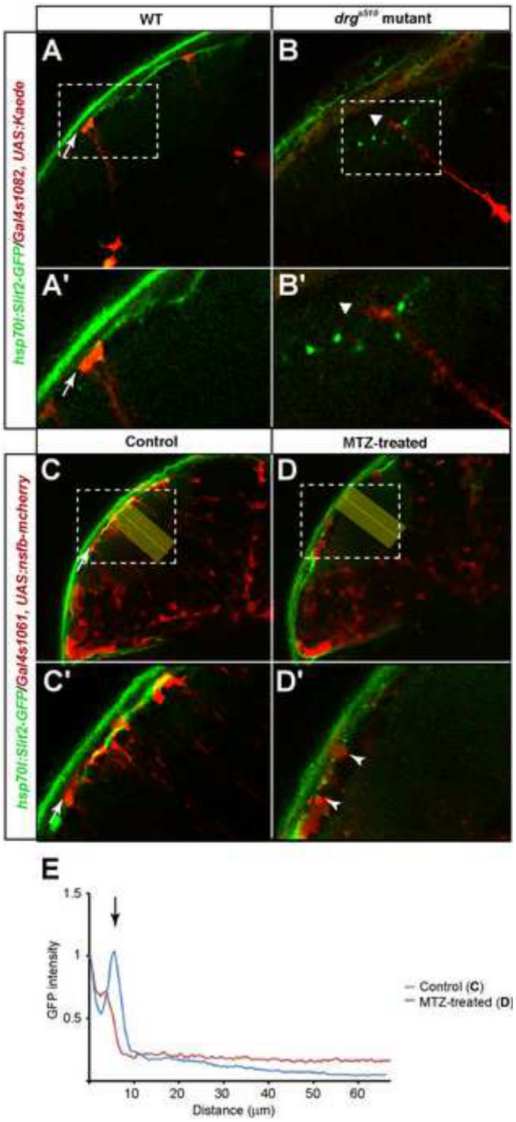

Figure 7. Radial glia are required for the surface localization of Slit in the tectum

Optical sections of 4 dpf *hsp70l:Slit2-GFP* tecta. Larvae were heat shocked at 79 hpf and imaged at 96 hpf. **A, B**. Radial glia were labeled with *Gal4*^{s1082t} and *UAS:Kaede*. Kaede was photoconverted to red. A' and B' show higher magnifications of the areas marked with dashed lines in A and B. Arrows point at radial glial endfeet in WT (A and A'). Triangles point at the distal ends of radial glia in *drg*^{s510} (B and B'). **C, D**. Radial glia were labeled with *Gal4s1061t* and *UAS:nfsbmCherry*. C shows control larva treated with 1% DMSO (C', higher magnification). D shows larva treated with 10mM MTZ (D', higher magnification). Arrows point at radial glial endfeet (C and C'). Arrowheads point at degenerated radial glia (D'). **E**. Densitometric plots of *Slit2:GFP* signal intensity from the areas indicated by yellow rectangles. Measurement and normalization as in Fig. 6M, N. Scale bar is 20 μm.